Physica A 560 (2020) 125126

Contents lists available at ScienceDirect

Physica A

journal homepage: www.elsevier.com/locate/physa

Delocalization and energy dynamics in a one-dimensional disordered nonlinear lattice

I.F.F. dos Santos [a], M.O. Sales [b], A. Ranciaro Neto [c], F.A.B.F. de Moura [a,*]

[a] Instituto de Física, Universidade Federal de Alagoas, 57072-970, Maceió - AL, Brazil
[b] IFMA Campus São João dos Patos, rua Padre Santiago, s/n, Centro, São João dos Patos-MA, 65665-000, Brazil
[c] Faculdade de Economia, Administração e Contabilidade, Universidade Federal de Alagoas, 57072-970, Maceió - AL, Brazil

ARTICLE INFO

Article history:
Received 24 December 2019
Received in revised form 14 August 2020
Available online 24 August 2020

Keywords:
Nonlinearity
Correlated disorder
Localization

ABSTRACT

We investigate the vibrational energy dynamics in classical nonlinear lattices with correlated random masses following a Fractionary Brownian motion sequence with power law spectrum proportional to $k^{-\alpha}$. In the absence of cubic interaction (the harmonic limit), we numerically demonstrate the existence of ballistic energy propagation at the limit of strong correlations ($\alpha > 2$). Calculations were done using numerical solution of the Hamilton's equations. When the cubic nonlinear interaction is added to our model, computation reveals the possibility of solitonic modes at the limit of strong correlations.

1. Introduction

The energy dynamics in classical nonlinear random lattices is a general interesting issue with direct connections with Anderson Localization [1–12]. With respect to disordered harmonic chains, it was shown that there are about $\sqrt{N}$ low-frequency non-localized modes, where N is the number of masses in the chain [1,2]. In Refs. [6–9,11] it was shown that high-frequency extended modes can be attained whenever the disorder distribution contains short or long-range correlations. Regarding thermal conductivity in classical lattices, the presence of nonlinearity also plays an important role on the energy flux [3,4,13–25]. In fact, the heat propagation in low dimensional classical nonlinear systems has been targeted by recent intense inquiry [14–19]. It is well known that nonlinear chains can, in general, exhibit kink-soliton solutions. However, the solitonic dynamics is damped by the presence of disorder. In fact, the scattering of solitons by disorder is measured by the reduction of localized energy within the localization region, by the time dependent acceleration of energy flux and by long-time behavior of the diffusion coefficient. The interplay between uncorrelated disorder and anharmonicity was studied in detail in Ref. [22]. It was numerically demonstrated that, while anharmonicity promotes energy transport through ultrasonic solitons, disorder decreases the propagation due to the well known Anderson localization [22]. The soliton dynamics in a Toda lattice with randomly distributed masses was studied in Ref. [23]. The disordered Toda's model consists of a one-dimensional chain of disordered masses where each one interacts with the others through a nearest-neighbor exponential potential. By using the inverse scattering transform, it was shown that the soliton energy decays as $\propto N^{3/2}$ for small-amplitude solitons and $\propto \exp(2N)$ for large-amplitude solitons [23]. In Ref. [24] the authors investigated the interplay between uncorrelated disorder and nonlinearity within the framework of the Fermi–Pasta–Ulam (FPU) model. It was demonstrated that at low temperatures, small system-size transport properties are dominated by disorder but the asymptotic system size dependence of current is given by the nonlinear interaction.

* Corresponding author.
E-mail address: fidelis@fis.ufal.br (F.A.B.F. de Moura).

https://doi.org/10.1016/j.physa.2020.125126
0378-4371/

In this work, we investigated the effect of a cubic nonlinearity on non-periodic classical lattices performing an numerical evaluation of the competition between correlated masses distribution and nonlinear cubic potentials. Long-range correlations within the masses distribution were imposed applying on them a Fractionary Brownian motion sequence with power law spectrum proportional to $k^{-\alpha}$. In the absence of anharmonic couplings, we employed numerical computation (finding solutions of Hamilton's equations) to demonstrate the existence of ballistic energy propagation at the limit of strong correlations ($\alpha > 2$). Taking into account the presence of cubic interaction, our results indicated that for strong correlations the ballistic dynamics is still achieved. Within this limit, although, our results reveals the presence of a solitonic like excitation.

2. Model and formalism

We consider a $1d$ anharmonic lattice of N masses, for which the classical Hamiltonian can be written as $H = \sum_n E_n(t)$, where the energy $E_n(t)$ of the mass at site (n) is given by [24–26]

$$E_n(t) = \frac{P_n^2}{2m_n} + \frac{1}{4}\Big[(Q_{n+1} - Q_n)^2 + (Q_n - Q_{n-1})^2\Big] + \frac{\eta}{6}\Big[(Q_{n+1} - Q_n)^3 + (Q_n - Q_{n-1})^3\Big] \tag{1}$$

Here P_n and Q_n define the momentum and displacement of the mass at site (n). In our model, m_n represents a quaternary correlated disorder distribution. We are using open boundary condition. We construct this sequence by mapping a continuous correlated series $\{V_n\}$ in a discrete group of four values (M_1, M_2, M_3, M_4). The continuous series $\{V_n\}$ is obtained by the trace of a fractional Brownian motion defined as [27–30]:

$$V_n = \sum_{k=1}^{N/2} \frac{1}{k^{\alpha/2}} \cos\left(\frac{2\pi nk}{N} + \phi_k\right). \tag{2}$$

Here, ϕ_k represent random phases distributed within the interval $[0, 2\pi]$. The above series have a power-law spectral density of the form $S(k) \propto 1/k^{\alpha}$ derived from the Fourier transform of the two-point correlation function. The widespread occurrence in nature of sequences with power-law noise is related to the general tendency of large dynamical systems to evolve to a self-organized critical state [31]. For $\alpha = 0$, the sequence is completely uncorrelated. Long-range correlated sequences are obtained in the regime $\alpha > 0$. According to the approach used in [27], we also performed a normalization process such that: $\langle V_n \rangle = 0$ and $\sqrt{\langle V_n^2 \rangle - \langle V_n \rangle^2} = 1$. Once the correlated sequence $\{V_n\}$ was built, we proceed to the mapping in order to generate the quaternary correlated sequence m_n. The mapping is defined by the equation below:

$$m_n = \begin{cases} M_1 & \text{if } V_n < -r_1 \\ M_2 & \text{if } -r_1 < V_n < r_2 \\ M_3 & \text{if } r_2 < V_n < r_3 \\ M_4 & \text{if } V_n > r_3. \end{cases} \tag{3}$$

The parameters r_1, r_2 and r_3 introduced into this expression controls the type of mapping we use. In general, r_1, r_2 and r_3 controls the probability of each of the four values (M_1, M_2, M_3, M_4) appearing on the quaternary distribution. We choose $0 < r_k < 1.5$ with $k = 1, 2, 3$, because 1.5 is close to the largest value of the V_n sequence after the normalization process. Moreover, we set the following values for the masses: $M_1 = 0.5$, $M_2 = 1.$, $M_3 = 1.5$, $M_4 = 2$. We emphasize that the transformation presented in Eq. (3) does not change drastically the statistical properties and correlations within the series $\{V_N\}$. In Fig. 1, we plot the autocorrelations $C_a(x)$ versus x for both series m_n and V_n. Such statistics are defined by $C_a(x) = (\langle a_n a_{n+x} \rangle - \langle a_n \rangle \langle a_{n+x} \rangle)/\sqrt{\langle a_n^2 \rangle - \langle a_n \rangle^2}$, with $a = m$ and V, respectively, for the m_n and V_n sequences. We observe that the correlations into m_n and V_n are roughly the same. In our calculations, we assume there is no disorder in the anharmonic contribution. By considering an initial excitation at the site n_0 at $t = 0$, we solve the differential equations for $P_n(t)$ and $Q_n(t)$ and compute the fraction of the total energy $H(t = 0)$ at the site n ($f_n = E_n(t)/H(t = 0)$). Therefore, we define the mean square displacement defined as: $\sigma(t) = \sqrt{[\sum_n (n - n_0)^2 f_n]}$. The time evolution of the width of the vibrational wave-packet (i.e $\sigma \propto t^A$) can be used to characterize the energy dynamics. If $A \approx 0$, then we have a fully localized wave-packet. If $A = 1$, the energy propagates ballistically along the lattice. If $A = 0.5$, the energy dynamics is diffusive. If $0 < A < 0.5$ the dynamics is sub-diffusive. The regime $0.5 < A < 1$ is called super-diffusive. In addition, we investigated the quantity defined as $Z(t) = (\sum_n^N f_n^2)$, where the inverse of Z measures the number of masses that participate of the energy transport. For localized states, $Z(t)$ is a constant along time and for extended states $Z(t)$ vanishes as $1/t$.

Within the Harmonic approximation ($\eta = 0$), it is possible to calculate the degree of localization by using the transfer matrix method (TMM). By considering $\eta = 0$ the Eq. (1) represents a harmonic chain of N masses in which that the equation of motion for the displacements $Q_n = u_n \exp i\omega t$ with vibrational frequency ω is [8,10]

$$(2 - \omega^2 m_n)u_n = u_{n-1} + u_{n+1} \quad . \tag{4}$$

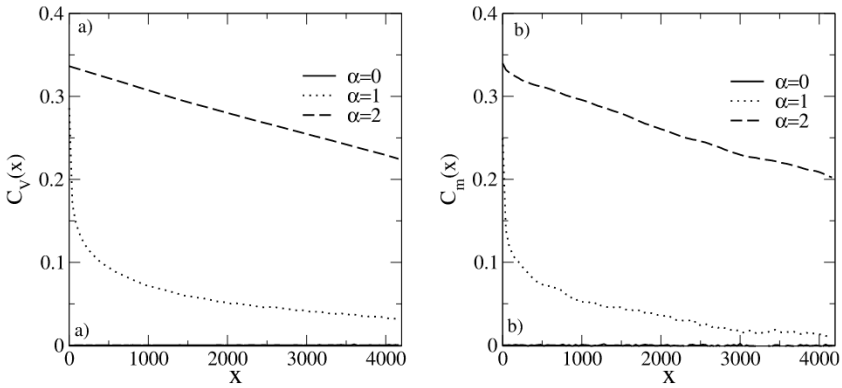

Fig. 1. The autocorrelations versus distance x for both series $\{m_n\}$ and $\{V_n\}$. We stress that autocorrelations are defined by $C_a(x) = (\langle a_n a_{n+x}\rangle - \langle a_n\rangle\langle a_{n+x}\rangle)/\sqrt{\langle a_n^2\rangle - \langle a_n\rangle^2}$ with $a = m$ and V respectively for the m_n and V_n sequences. We observe that the autocorrelations into m_n and V_n are roughly the same. Therefore, the discretization of the series $\{V_n\}$ in a Quaternary sequence does not change drastically the intrinsic statistical properties.

The TMM is obtained by using a matrix recursive reformulation of the scaled displacement equation Eq. (4)

$$\begin{pmatrix} u_{n+1} \\ u_n \end{pmatrix} = \begin{pmatrix} 2 - m_n\omega^2 & -1 \\ 1 & 0 \end{pmatrix} \begin{pmatrix} u_n \\ u_{n-1} \end{pmatrix} . \tag{5}$$

For a specific frequency ω, a 2×2 transfer matrix T_n connects the displacements at the sites $n-1$ and n to those at the site $n+1$. Once the initial values for u_0 and u_1 are known, the value of u_n can be obtained by repeated iterations along the chain, as described by the product of transfer matrices

$$Y_N = \prod_{n=1}^{N} T_n. \tag{6}$$

The Lyapunov exponent γ (the inverse of the localization length) of each vibrational mode is defined by [8,10]

$$\gamma = \lim_{N\to\infty} \frac{1}{N} \log \frac{|Y_N c(0)|}{|c(0)|}, \tag{7}$$

where $c(0) = \binom{u_1}{u_0}$ is a generic initial condition. Typically, 10^7 matrix products were used to calculate the localization length. For localized eigenmodes we have $\gamma > 0$ and for extended ones the Lyapunov exponent trends to zero.

3. Results

We initially analyzed the harmonic case i.e $\eta = 0$ considering a system size of $N = 25\,000$ and an initial impulse excitation at the center of chain (i.e. $Q_n = 0$ and $P_n = v_0\delta_{n,N/2}$). The Hamilton equations were solved using a standard Fourth order Runge–Kutta [32] with $dt = 5 \times 10^{-4}$. The total energy $H(t) = \sum_n E_n(t)$ was analyzed over time in order to check the accuracy of our numerical solution. In our calculations, the quantity $R(t) = |1 - H(t=0)/H(t)|$ was less than 10^{-10} along the entire time interval. In Fig. 2, we plot the mean square displacement $\sigma(t)$ versus time for $\eta = 0$, $\alpha = 0$, 1 and 3 and $r_1 = 1$, $r_2 = 0.1$ and $r_3 = 1.2$. Our results showed that for $\alpha = 0$ and 1 the energy propagates in a super-diffusive way ($\sigma(t) \propto t^{3/4}$). These results were consistent with the previous one for the vibrational energy dynamics in disordered classical harmonic chains [8]. For $\alpha = 3$, the calculations pointed to the ballistic energy propagation along the chain (i.e $\sigma(t) \propto t^1$). We stress that this result was obtained using a quaternary sequence with strong long-range correlations. However, ballistic propagation in classical chains with long-range correlations was previously reported in Ref. [8]. The main difference between our results and those reported in [8] is the type of masses distribution (the disordered masses distribution considered in [8] was a sequence chosen in an interval $[m_o, m_f]$). In Figs. 3, 4 we plot a wide collection of results for $\sigma = \sigma(t \to \infty)$ and $Z = Z(t \to \infty)$ versus α for several values of r_1, r_2 and r_3. In order to calculate $\sigma(t \to \infty)$ and $Z(t \to \infty)$ we solved the Hamilton equations for a very long time ($t_{max} \approx 4N$) and then calculate the both quantities as: $\sigma(Z)(t \to \infty) = \sum_{t=t_1}^{t_{max}} \sigma(Z)(t)/N_t$ where t_1 was about $0.75t_{max}$ and N_t is the number of times between t_1 and t_{max}. To perform a finite size analysis, we plot σ/N and ZN as both quantities, for extended states, become approximately independent of N. In Figs. 3, 4, we note that for $\alpha > 2$, the data for both σ and Z indicate the presence of extended states regardless r_1, r_2, r_3 values.

In order to verify the existence of extended eigenmodes for $\alpha > 2$ at the limit of large size, we applied the transfer matrix formalism (TMM). In Fig. 5(a) we show computation of the Lyapunov exponent versus square frequency for $\alpha = 0$, 1, 3 and $N = 10^7$. Our calculations indicate that, for $\alpha = 3$, there is a range of frequencies ($[0, \omega_c]$ with $\omega_c > 0$)

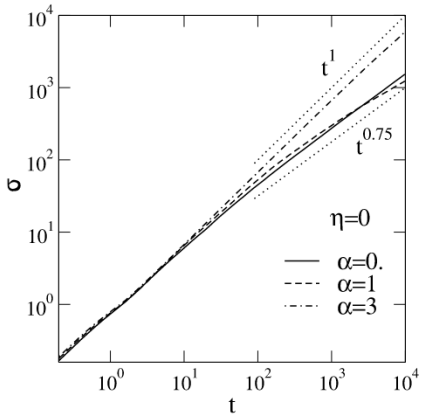

Fig. 2. $\sigma(t)$ versus time t for $\eta = 0$, $\alpha = 0$, 1 and 3 and $r_1 = 1$, $r_2 = 0.1$ and $r_3 = 1.2$. Our results showed that, for $\alpha = 0$ and 1, the energy propagates in a super-diffusive way ($\sigma(t) \propto t^{3/4}$). For $\alpha = 3$, the calculations indicate that the energy propagates ballistically along the chain (i.e $\sigma(t) \propto t^1$).

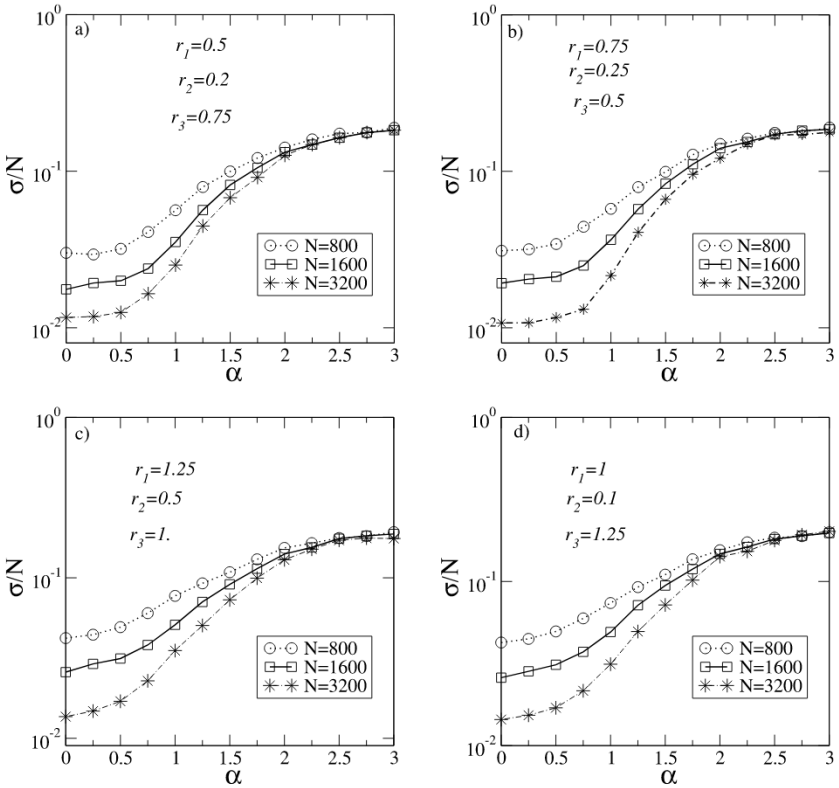

Fig. 3. Scaled mean square displacement for $t \gg 0(\sigma/N = \sigma(t \to \infty)/N$ versus α for several values of r_1, r_2 and r_3. Calculations indicated that, for $\alpha > 2$, the mean square displacement diverges linearly with N thus pointing to extended states.

in which the Lyapunov exponent is vanishing. For $\alpha < 2$, the Lyapunov is zero only for $\omega = 0$ (see inset of Fig. 5(a)). In Fig. 5(b), we plot mean Lyapunov exponent $\langle\gamma\rangle$ versus α for $N = 10^7$. The expression for the mean Lyapunov exponent is $\langle\gamma\rangle = \sum_{\omega_1^2<\omega^2<\omega_2^2} \gamma(\omega^2)$ with $\omega_1^2 = 0.2$ and $\omega_2^2 = 0.5$. Our calculation indicate that, for $\alpha > 2$, a phase of extended eigenmodes has occurred with non-zero frequencies (in good agreement with the results showed in Figs. 3 and 4).

When including the nonlinear interaction to the system, our results were interesting and completely counter-intuitive. In Fig. 6 we plot both quantities ($\sigma(t)$ and $Z(t)$ versus time for $\alpha = 3$ and $\eta = 0.5$ and 1.0. Assessing mean square displacement we observed that, no matter values η may assume, the energy propagation seems to keep its ballistic dynamics ($\sigma(t) \propto t^1$). Therefore, after computation, energy flux in both harmonic or unharmonic chain with correlated

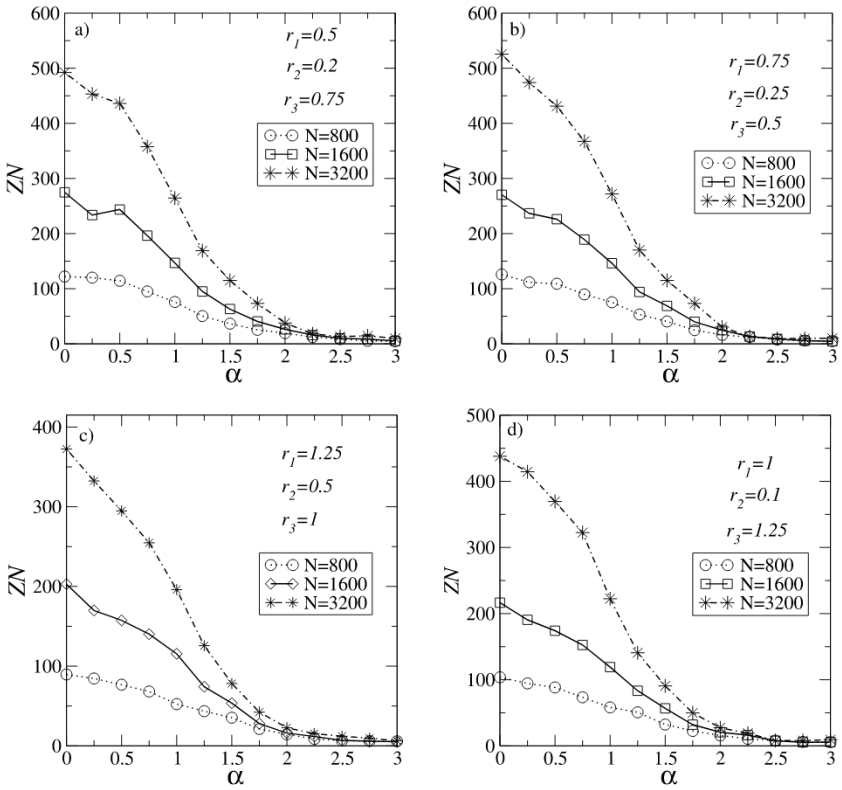

Fig. 4. Scaled Z function for long time ($ZN = Z(t \to \infty)N$) versus α for several values of r_1, r_2 and r_3. In accordance with the calculations showed in Fig. 3, we found that, for $\alpha > 2$, the Z function scales as $1/N$, a clear signal of metallic states.

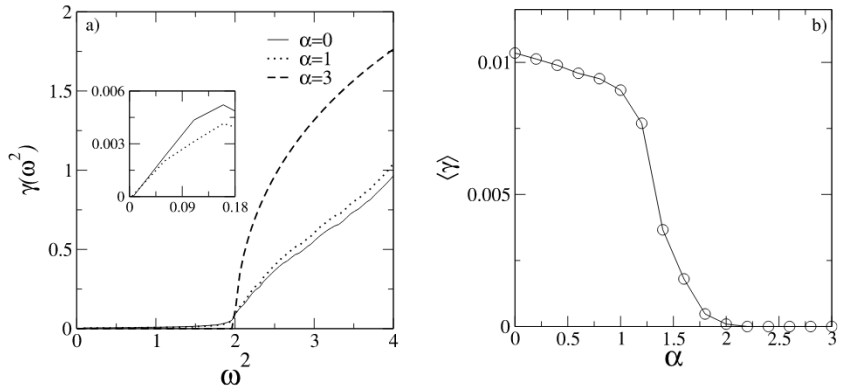

Fig. 5. (a) Lyapunov exponent versus ω^2 for $\alpha = 0$, 1, 3 and $N = 10^7$. Our calculations indicate that, for $\alpha = 3$, there is a phase of extended vibration modes within the interval $[0, \omega_c]$ with $\omega_c > 0$; the cases with $\alpha < 2$ indicate that the Lyapunov is zero only for $\omega = 0$ (see inset). (b) The mean Lyapunov $\langle\gamma\rangle$ within the interval $[\omega_1^2 = 0.2, \omega_2^2 = 0.5]$ versus α for $N = 10^7$. Calculations indicate that for $\alpha > 0$ there are extended states within this model (in good agreement with the results showed in Figs. 3 and 4).

disorder exhibits a fast propagation. However, by analyzing the time evolution of the Z function we found a curious result: the Z function behaves roughly as constant. We stress that for $\alpha = 3$ and $\eta = 0$ we dealt with the limit that metallic states are present, and, for $\alpha = 3$ and $\eta > 0$, we note a ballistic regime, based on the results of $\sigma(t)$. However, the strange behavior of $Z(t)$ is inconsistent with existence of extended states. In order to understand asymmetric behavior of Z function better, an evaluation of energy spacial profile using a 3d-plot (n, t, E_n) (see Fig. 7(a–d)) was carried. We highlight that, within these figures of the energy profile, we considered $n = 0$ as the center of chain. Computation was done in a chain with $N = 2000$, $\alpha = 3$, $r_1 = 1$, $r_2 = 0.1$ and $r_3 = 1.2$ and the initial condition was $Q_n(t = 0) = 0$ and $P_n(t = 0) = v_0\delta_{n,0}$. For $\alpha = 3$ and $\eta = 0$ (see Fig. 7(a) with $v_0 = 1$), we found that the energy profile was in good correspondence with previous works (see [8,21,22]). The initial energy impulse spreads ballistically in both directions.

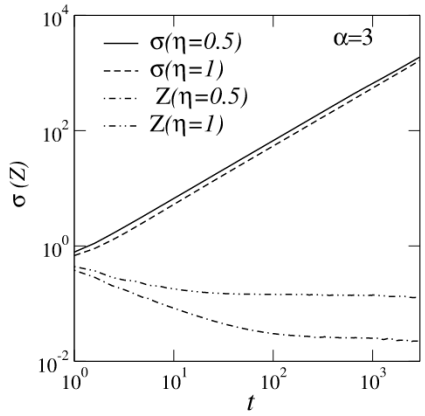

Fig. 6. The time evolution of $\sigma(t)$ and $Z(t)$ for $\alpha = 3$ and $\eta = 0.5$ and 1.0. The results of the mean square displacement show that, regardless the value of η considered, the energy propagates ballistically ($\sigma(t) \propto t^1$). However, in contrast to the results obtained for mean square displacement, the Z function behaves roughly as constant.

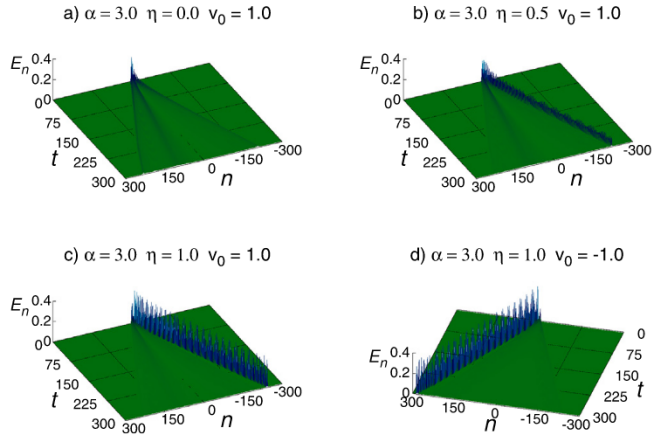

Fig. 7. Energy spacial profile using a 3d-plot (n, t, E_n) for several valuers of η (here $n = 0$ as the center of chain). The initial condition was an impulse excitation at the center of chain i.e. $Q_n(t = 0) = 0$ and $P_n(t = 0) = v_0\delta_{n,0}$.

Nevertheless, when $\eta > 0$ (Fig. 7(b,c) with $v_0 = 1$), the energy exhibits a solitonic like profile similar to the one found in periodic nonlinear chains [21,22]. Therefore, the nonlinearity, even at the presence of correlated disorder, promotes the appearance of stable solitonic-like excitation. It is instructive, for example, to check the dependence of this solitonic mode with the signal of initial impulse. In Fig. 7(c), we have the energy profile imputing $\alpha = 3$, $\eta = 1$ and $v_0 = -1$; the observed direction of solitonic dynamics is inverted (a) standard property associated with solitonic like excitation [21,22]). The asymmetric behavior of Z function can be now explained using some additional tools namely $Z_{+(-)} = \sum_{n_{+(-)}} f_n^2$. n_+ represents the region with $n > N/2$ and n_-, the region with $n < N/2$. Therefore, Z_+ represents the image set of Z function for $n > 0$ (i.e the positive side of the energy profile). The explanation of Z_- is symmetric: Z_- is the image of Z function for $n < 0$ (i.e the negative side of the energy profile). The results for $Z_{+(-)}$ versus time can be found in Fig. 8. The initial condition used here was $Q_n(t = 0) = 0$ and $P_n(t = 0) = v_0\delta n, 0$ with $v_0 = 1$. For $\eta = 0$, both quantities (Z_+ and Z_-) exhibit a linear decay ($Z_{+(-)} \propto 1/t$) in agreement with the existence of extended states and the ballistic spread obtained in $\sigma(t)$. However, for $\eta > 0$ the asymmetric solitonic energy profile imposes distinct dynamics for Z_+ and Z_-. On the positive side, the energy spreads ballistically, therefore Z_+ behaves as $1/t$. On the other hand, on the negative side we have a solitonic mode thus a finite fraction of the initial energy remains trapped along the time (see Z_- distribution over time).

When $\alpha < 2$, energy dynamics should be analyzed. In Fig. 9(a–d) we plot the energy spatial profile for $\alpha = 0$ and 1 and $\eta = 0$ and 1. Calculations were done in a chain with $N = 2000$, $r_1 = 1$, $r_2 = 0.1$ and $r_3 = 1.2$ and the initial condition was $Q_n(t = 0) = 0$ and $P_n(t = 0) = \delta_{n,0}$. For $\eta = 0$ we note that a portion of the initial energy remains trapped around the initial position while the other fraction spreads along the chain. For $\eta = 1$, we see that in both cases ($\alpha = 0$ and 1) we have a merge of both dynamics: there is a portion of the initial energy trapped around the initial site and also an apparent solitonic like excitation propagating within the negative side (moreover, there is some small radiations spreading in both

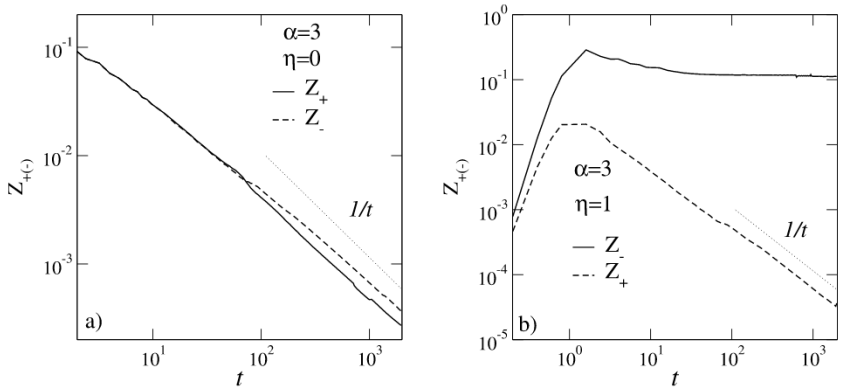

Fig. 8. The Z function calculated separately on the positive and negative sides of Fig. 7(a) (i.e $Z_{+(-)}(t) = \sum_{n_{+(-)}} f_n^2$).

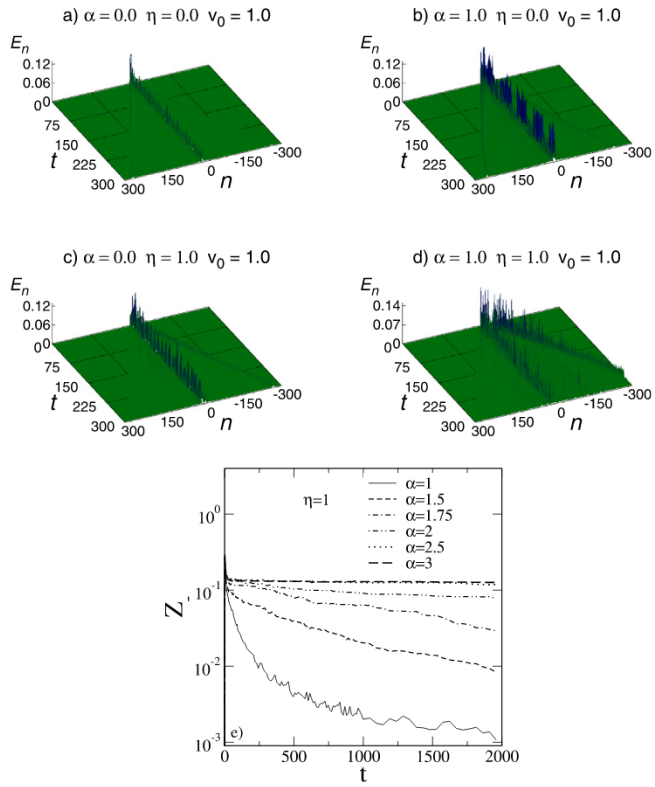

Fig. 9. (a–d) The energy spatial profile for $\alpha = 0$ and 1 and $\eta = 0$ and 1. Calculations were done in a chain with $N = 2000$, $r_1 = 1$, $r_2 = 0.1$ and $r_3 = 1.2$ and the initial condition was $Q_n(t = 0) = 0$ and $P_n(t = 0) = \delta_{n,0}$. (e) Z function within the negative side.

directions of the chain). For $\alpha = 1$ the solitonic like mode is more visible that in the case with $\alpha = 0$. However, the lifetime of this solitonic mode is too short. Even within this 3d plot, the magnitude of the apparent soliton decreases as the time is increased. In order to clarify this point we calculate the Z function within the negative side considering $r_1 = 1$, $r_2 = 0.1$ and $r_3 = 1.2$ and $\eta = 1$ (i.e Z_-, see Fig. 9(e)). For $\alpha < 2$ and $\eta = 1$, the Z_- decreases with time − consistent with the damped of the solitonic intensity observed in Fig. 9(c,d). For $\alpha > 2$, we observed that Z_- remains constant thus suggesting the stability of the solitonic mode found within this limit. The main explanation for this phenomenon is the existence of extended states within the band of allowed states. The presence of states that propagate ballistically associated with the cubic interaction promote the occurrence of a solitonic mode without any damping. Conversely, because the case with $\alpha < 2$ does not contain extended states, nonlinear excitation is destroyed.

Lastly, we show a short analysis about the dependence of the soliton formation with the initial velocity v_0. In Fig. 10 we plot the participation function at the negative side of the energy profile (i.e Z_-) computed considering $Q_n(t = 0) = 0$ and

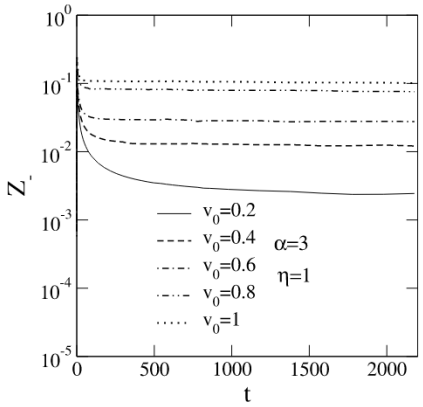

Fig. 10. Participation function computed for $n < N/2$ (i.e Z_-). Calculations were done considering $Q_n(t = 0) = 0$, $P_n(t = 0) = v_0\delta_{n,N/2}$, $r_1 = 1$, $r_2 = 0.1$ and $r_3 = 1$, $\eta = 1$, $\alpha = 3$ and $N = 25\,000$ sites. Our calculations indicate that as the velocity is decreased the intensity of soliton peak also decreases.

$P_n(t = 0) = v_0\delta_{n,N/2}$, $r_1 = 1, r_2 = 0.1$ and $r_3 = 1$, $\eta = 1$ and $\alpha = 3$. Calculations were done in large chain with $N = 20\,000$ sites resulting that, for $v_0 > 0$, the solitonic model is observed. However, as the velocity is decreased, the amount of energy within the soliton also decreases. Analogously, as the initial velocity is decreased, the initial energy into the chain also decreases thus lowering the amount of initial energy captured by nonlinear excitation. Consequently, intensity of the solitonic peak diminishes. We emphasize that we found no dependence of the velocity of soliton propagation with the initial velocity v_0.

4. Summary

We have investigated the competition between correlated disorder and cubic nonlinearity in a classical chain. Our model was a FPU model with correlated disorder at the masses distribution. For the construction of a long-range correlated masses sequence, we use a random series with a power law spectrum. In the absence of anharmonic couplings, we numerically demonstrated the existence of ballistic energy propagation at the limit of strong correlations. The inclusion of cubic interaction did not destroy the ballistic propagation. However, the energy profile exhibits a solitonic like mode that propagates without any damping.

CRediT authorship contribution statement

I.F.F. dos Santos: Conceptualization, Methodology and numerical calculations of figs. 2,3,4. **M.O. Sales:** Software, Validation, Writing - original draft. **A. Ranciaro Neto:** Data curation, Writing - original draft. **F.A.B.F. de Moura:** Conceptualization, Methodology, Software, Numerical calculations of figs. 1,5-10, Writing - original draft.

Declaration of competing interest

The authors declare that they have no known competing financial interests or personal relationships that could have appeared to influence the work reported in this paper.

Acknowledgments

This work was partially supported by CNPq, Brazil, CAPES, Brazil, and FINEP, Brazil (Federal Brazilian Agencies), CNPq-Rede Nanobioestruturas, as well as FAPEAL (Alagoas State Agency).

References

[1] P. Dean, Proc. Phys. Soc. 84 (1964) 727.
[2] H. Matsuda, K. Ishii, Progr. Theoret. Phys. Suppl. 45 (1970) 56;
K. Ishii, Prog. Theor. Phys. Suppl. 53 (1973) 77.
[3] P.L. Garrido, P.I. Hurtado, B. Nadrowski, Phys. Rev. Lett. 86 (2001) 5486.
[4] Abhishek Dhar, Phys. Rev. Lett. 86 (2001) 5882.
[5] Y. Zhang, H. Zhao, Phys. Rev. E 66 (2002) 026106.
[6] F. Domínguez-Adame, E. Maciá, A. Sánchez, Phys. Rev. B 48 (1993) 6054.
[7] P.K. Datta, K. Kundu, J. Phys.: Condens. Matter 6 (1994) 4465.
[8] F.A.B.F. de Moura, M.D. Coutinho-Filho, E.P. Raposo, M.L. Lyra, Phys. Rev. B 68 (2003) 012202.

[9] S.S. Albuquerque, F.A.B.F. de Moura and, M.L. Lyra, Physica A 357 (2005) 165.
[10] F.A.B.F. de Moura, L.P. Viana, A.C. Frery, Phys. Rev. B 73 (2006) 212302.
[11] F.A.B.F. de Moura, F. Domínguez-Adame, Eur. Phys. J. B 66 (2008) 165.
[12] F.A.B.F. de Moura, J. Phys.: Condens. Matter 22 (2010) 435401.
[13] S. Lepria, R. Livi, A. Politi, Phys. Rep. 377 (2003) 1.
[14] G.S. Zavt, M. Wagner, A. Lütze, Phys. Rev. E 47 (1993) 4108.
[15] P.K. Datta, K. Kundu, Phys. Rev. B 51 (1995) 6287.
[16] B. Li, H. Zhao, B. Hu, Phys. Rev. Lett. 86 (2001) 63;
A.V. Savin, G.P. Tsironis, A.V. Zolotaryuk, Phys. Rev. Lett. 88 (2002) 154301-1;
A. Dhar, Phys. Rev. Lett. 88 (2002) 249401-1;
P.L. Garrido, P.I. Hurtado, Phys. Rev. Lett. 88 (2002) 249402-1;
B. Li, J. Wang, Phys. Rev. Lett. 91 (2003) 044301.
[17] M.M. Sano, K. Kitahara, Phys. Rev. E 64 (2001) 056111.
[18] A.V. Savin, G.P. Tsironis, A.V. Zolotaryuk, Phys. Rev. Lett. 88 (2002) 154301-1.
[19] B. Li, L. Wang, B. Hu, Phys. Rev. Lett. 88 (2002) 223901.
[20] R. Orbach, Phil. Mag. B 65 (1992) 289.
[21] M. Wagner, G. Zart, J. Vazquez-Marquez, G. Viliani, W. Frizzera, O. Pilla, M. Montagna, Phil. Mag. B 65 (1992) 273.
[22] G.S. Zavt, M. Wagner, A. Lütze, Phys. Rev. B 47 (1993) 4108.
[23] J. Garnier, F. Kh. Abdullaev, Phys. Rev. E 67 (2003) 026609.
[24] Abhishek Dhar, Keiji Saito, Phys. Rev. E 78 (2008) 061136.
[25] Trieu Mai, Abhishek Dhar, Onuttom Narayan, Phys. Rev. Lett. 98 (2007) 184301.
[26] E. Fermi, J.R. Pasta, S.M. Ulam, Los Alamos Report No LA-(1955), 1940.
[27] F.A.B.F. de Moura, M.L. Lyra, Phys. Rev. Lett. 81 (1998) 3735.
[28] F.A.B.F. de Moura, M.D. Coutinho-Filho, E.P. Raposo, M.L. Lyra, Europhys. Lett. 66 (585) (2004).
[29] I.F. dos Santos, F.A.B.F. de Moura, M.L. Lyra, M.D. Coutinho-Filho, J. Phys.: Condens. Matter 19 (2007) 476213.
[30] F. Domínguez-Adame, V.A. Malyshev, F.A.B.F. de Moura, Lyra M. L., Phys. Rev. Lett. 91 (2003) 197402.
[31] P. Bak, C. Tang, K. Wiesenfeld, Phys. Rev. Lett. 59 (1987) 381.
[32] E. Hairer, S.P. Nørsett, G. Wanner, Solving ordinary dierential equations I: Nonstiff problems, in: W.H. Press, B.P. Flannery, S.A. Teukolsky, W.T. Wetterling (Eds.), Springer Series in Computational Mathematics, third ed., in: Numerical Recipes: The Art of Scientific Computing, Cambridge University Press, New York, 2007.